TWO-COMPONENT PROPELLANT GRAIN FOR ROCKET MOTOR
Combustion Analysis and Geometric Optimization

by

Mohammed ALAZEEZI*, Nikola P. POPOVIĆ, and Predrag M. ELEK

Faculty of Mechanical Engineering, University of Belgrade, Belgrade, Serbia

Original scientific paper
https://doi.org/10.2298/TSCI210604290A

The paper considers utilization of rocket motor propellant grains that consist of two propellants. The idea is to achieve approximately neutral burning using an outer surface inhibited cylindrical shape and complex contact surface between propellants. An existing propellant grain with complex geometry has been analytically modeled in terms of determination of evolution of corresponding burning surface areas. The analytical and experimental results' diagrams of this grain have been found to have a saw-tooth shape because of the segments that separate the two propellants, causing potential problems in the burning process during the relatively short active phase, showing an obvious need for further optimization. This has created an opportunity for development of improved propellant grain geometry and corresponding mathematical model for determination of main interior ballistic parameters. Comparison between calculation results based on both models and experimentally determined chamber pressure data shows very good agreement. Therefore, two-component propellant grains have significant application possibilities using the suggested modeling approaches.

Key words: *rocket propulsion, solid propellant, grain geometry, optimization, two-component grain*

Introduction

Solid propellant rocket motors (SPRM) have found their use in a plethora of different scientific and commercial fields due to their simplicity, reliability, and they require little servicing [1]. This growing practical usage has led SPRM to be considered one of the most reliable and cost-effective propulsion systems for rocket-based applications, ranging from minor tactical weapons to large scale space mission rockets [2]. A large number of manufacturers and designers prefer and even suggest the use of SPRM, rather than other variants of propulsion systems, due to their relatively simple design, simplified manufacturing process, long lifetime, easy storage, readiness for use and low cost [3]. Generally, a solid propellant rocket motor may consist of five main components as illustrated in fig. 1. These components are the nozzle, igniter, insulation, metal structure or case and the propellant grain which has the highest impact towards the performance of the motor [5].

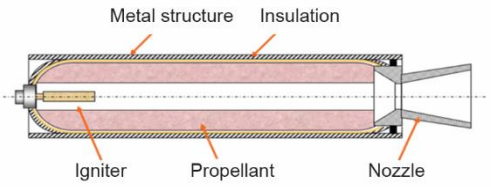

Figure 1. Illustration of SPRM components [4]

* Corresponding author, e-mail: malazizi90@gmail.com

Solid rocket propellants consist of fuel and oxidizer that react chemically under certain conditions to release energy, thereby producing thrust. In SPRM, the amount of produced thrust depends on the propellant's composition, shape and the design of the nozzle. In terms of design optimization and efficiency, many researchers have been conducting intensive work in the past few decades. The importance of automated design of solid rocket propellant systems was conducted and demonstrated in [6]. The research was limited due to the under-developed computational methods.

The SPRM are designed in line with mission requirements set before them, predetermined by the rocket's application. Upon establishing the mission type, it is essential to define a desired thrust profile. After selecting an appropriate propellant composition, the main design variable or parameter affecting the thrust profile will be the grain geometry [7-11]. The change of grain geometry during operation of the SPRM defines the burned surface area for an amount of web. This process is called burnback analysis of solid propellant grains. It is important to take into account the change of the burning surface area as an essential parameter for the interior ballistics' calculations and prediction of SPRM performance parameters [12]. The propellant grain has a burning that regresses in a direction perpendicular to the burning surface. The rate of regression is the burning rate r, which is usually expressed by the formula given by Saint Robert and Vieille [13]:

$$r = bp_0^n \tag{1}$$

Another important parameter in the interiors ballistics is the mass-flow rate which is determined by the following equation:

$$\dot{m} = A\rho_\mathrm{p} r \tag{2}$$

The characteristic velocity, c^*, is a function of the propellant characteristics and combustion chamber design, and it is essentially independent of the nozzle characteristics. It is defined as the product of chamber pressure and nozzle throat area divided by the propellant mass flow rate and can be expressed:

$$c^* = \frac{p_0 A_\mathrm{t}}{\dot{m}} = \frac{\sqrt{\mathrm{R}T_\mathrm{c}}}{\gamma} \tag{3}$$

where parameter γ is:

$$\gamma = \sqrt{k}\left(\frac{2}{k+1}\right)^{\frac{k+1}{2(k-1)}} \tag{4}$$

Assuming homogeneous chamber pressure and steady-state process, the equilibrium chamber pressure, p_0, can be determined by balancing the mass-flow rate of the generated gas from eq. (2), and its mass-flow rate through the nozzle defined by (3):

$$p_0 = \left(b\rho_\mathrm{p} c^* \frac{A}{A_\mathrm{t}}\right)^{\frac{1}{1-n}} \tag{5}$$

The chamber pressure could be influenced by the change of initial temperature of the propellant grain ΔT_b, and that effect on the motor pressure could be expressed:

$$p = p_0 \exp(\pi \Delta T_\mathrm{b}) \tag{6}$$

where π is the temperature sensitivity of the pressure, and it is calculated as shown in eq. (7) as the function of the burn rate exponent n and the temperature sensitivity of the burning rate, σ_p.

$$\pi = \frac{1}{1-n}\sigma_p \tag{7}$$

In the case of a two-component propellant grain, the total generated mass-flow rate is equal to the mass-flow rate through the nozzle:

$$\dot{m}_f + \dot{m}_s = \dot{m} \tag{8}$$

Using eqs. (1) and (2), this condition can be written in the equivalent form:

$$\rho_f A_f b_f p^{n_f} + \rho_s A_s b_s p^{n_s} = \frac{pA_t}{\bar{c}^*} \tag{9}$$

where $\bar{c}^*$ is the average characteristic velocity of the mixture of combustion products. Using the calculated values of the burning surface areas A_f and A_s and having in mind that other parameters are propellant properties, the equilibrium pressure can be numerically calculated from eq. (9). Therefore, during the evolution of the combustion of a two-propellant grain, in the case when only one propellant burns the operating chamber pressure is determined from eq. (5), otherwise, eq. (9) is used.

The previously listed parameters are all necessary when creating a precise model of a rocket motor and using them it is possible to calculate values that dictate the performance of the selected motor configuration.

Burnback phenomenology of two-component grain is considered through analysis and optimization of an existing SPRM with a complex grain consisting of two propellants. The optimized model will serve the purpose of simplifying the grain's shape while delivering the same performance. The grain's shape will be altered in order to have a simpler configuration than the original model. The process of the burnback analysis and performance calculations could be carried out in a programmed code or software to deliver accurate and reliable results as the code that was developed in [14]. In this project, a MATLAB code is developed to incorporate the original and optimized grain's mathematical models, along with their interior ballistics, in order to deliver a comparison of the performance parameters.

Burnback analysis of two-component propellant grain

This type of grain consists of two propellants, one of which has a higher burning rate than the other. They are composite solid propellants that have similar compositions but a different oxidizer and fuel ratios. The propellants are based on ammonium perchlorate (AP), as an oxidizer, and significant experimental work has been done to find out the parameters that influence the burning rates of compositions that contain AP [15, 16]. The propellants composition will not be discussed in this paper as its characteristics will be introduced in the model as a given input. However, it is an area of interest to study the selected propellant of this grain.

The grain's cylindrical shape was set as a requirement, as well as a neutral thrust profile. Therefore, this requirement could be fulfilled through two solutions, which will be discussed.

Original propellant grain

The existing (original) grain consists of two propellants that give the final configuration of a cylindrical grain. The geometry of the original grain with characteristic stepped contact surface between two propellants is shown in fig. 2. The outer cylindrical surface and the left frontal area are inhibited where the right side is open to the nozzle. Due to the complex geometry of contact surface between the propellants, the burnback analysis will consist of multiple steps that represent the burning surface area at each burned web.

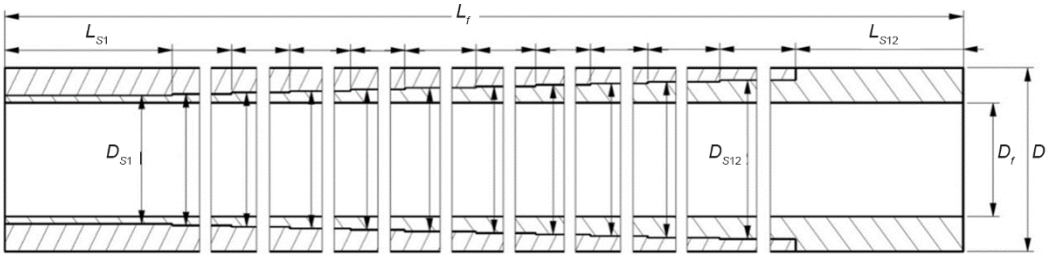

Figure 2. Geometry of the original two-propellant grain

The burnback process is described analytically and implemented in MATLAB using multiple loops for calculating the output parameters at each step during the burning process.

Initial step

In this step, the burning is occurring only in the fast burning propellant. The burning surface area consists of the cylindrical inner tube, combined with the frontal ring shaped area. The initial tube length is marked as L_f and represents the total length of the tube. The grain's web thickness is defined by the interior diameter of the tube D_f and the total exterior diameter of the grain D. This step concludes after the interior diameter D_f reaches a value equal to the interior diameter of the first step of the slow burning propellant D_{s1}. The following relations demonstrate the burning surface area:

$$A_f = \pi L_{f(k)} D_{f(k)} + \frac{\pi}{4}[D^2 - D_{f(k)}^2] \tag{10}$$

$$L_{f(k+1)} = L_{f(k)} - w \tag{11}$$

$$D_{f(k+1)} = D_{f(k)} + 2w \tag{12}$$

$$A_s = 0 \tag{13}$$

where A_f is the burning surface area of the fast burning grain, A_s – the burning surface area of the slow burning fuel, L_f – the current length of grain, numerically lowered in each iteration by a predefined parameter, w, forming L_{f1} at the end of the first burning step. The burned web w determines how fine each iteration step will be. Due to parameter D_f being related to the grain burn rate in the same way as L_f, it is also calculated in each iteration using w. The currently running iteration is represented with the index k, while the upcoming next iteration is marked with $k+1$.

General step

In this step, the burning will start spreading to the slow burning propellant, therefore, the following relations demonstrate the burning surface area that progressing at both propellants:

$$A_{\mathrm{f}} = \pi L_{\mathrm{f}(k)} D_{\mathrm{f}(k)} + \frac{\pi}{4}[D^2 - D_{\mathrm{f}(k)}^2] + \sum \pi L_{\mathrm{f}(i)(k)} D_{\mathrm{f}(i)(k)} \tag{14}$$

$$L_{\mathrm{f}(i)(k+1)} = L_{\mathrm{f}(i)(k)} - w \tag{15}$$

$$D_{\mathrm{f}(k+1)} = D_{\mathrm{f}(k)} + 2w \tag{16}$$

$$A_{\mathrm{s}} = \pi L_{\mathrm{s1}} D_{\mathrm{s1}} + A_{\mathrm{s1}e} \tag{17}$$

$$A_{\mathrm{s1}e} = \pi[D_{\mathrm{f}(k)} + D_{\mathrm{s1}(k)}]\frac{e_1}{2} \tag{18}$$

where index i represents the number of the step. During burning, each time the burning front reaches a new step, a new shape will begin forming at the edge of each slow burning grain step, due to the difference in burning rates. This step causes the propellant to not only burn in the radial and axial or longitudinal direction. This new shape is viewed as a slope and can be calculated for each step in order to further increase the accuracy of the mathematical model. Equations of the burned edge as a new step are:

$$D_{\mathrm{s1}(k+1)} = D_{\mathrm{s1}(k)} + 2w\frac{r_2}{r_1} \tag{19}$$

$$a_{1(k+1)} = a_{1(k)} + w\frac{r_2}{r_1} \tag{20}$$

$$c_{1(k+1)} = c_{1(k)} + w \tag{21}$$

$$e_{1(k+1)} = \sqrt{a_{1(k+1)}^2 + [c_{1(k+1)} - a_{1(k+1)}]^2} \tag{22}$$

$$L_{\mathrm{s1}(k+1)} = L_{\mathrm{s1}(k)} - a_{1(k+1)} \tag{23}$$

where D_{s1} represents the interior diameter of the slow burning propellant first step. If the difference of burning speeds is taken into consideration, in order to calculate the area of the newly forming slope, it is necessary to introduce parameters a and c, representing axial and radial burning of the edge of the step, respectively, as shown in fig. 3. Through them one can calculate e, which is the length of a single slope.

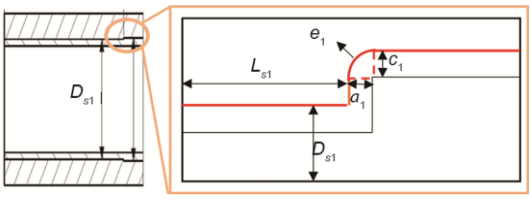

Figure 3. An illustration on the new formed step

Optimized grain geometry

The original propellant grain configuration was designed in such a way due to the manufacturing limitations. Multiple methods and techniques were developed by the researchers in this field for designing and optimizing solid propellant grain shapes [17-19]. Thus, an optimization model has been developed for this project to reduce the complexity of the grain's shape while keeping the same performance outputs. The optimized model is consisted of five burning phases that will go through the two propellants, as shown in fig. 4. The mathematical model will be shown only for Phase 3 as it is the most complex one, and hence the burnback analysis for the other phases are simpler and could be calculated in an analogous way.

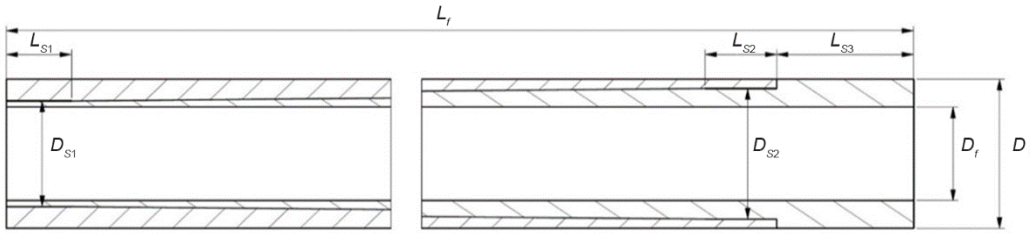

Figure 4. Geometry of the optimized model

Phase 1. The first phase of the burning will be identical to the original model as shown in fig. 5, meaning that it will just evolve through the fast burning propellant from D_f to D_{s1}, and from L_{f0} to L_{f1} from the right side. The burning surface area equations of the first phase are similar to the set of eqs. (10)-(13).

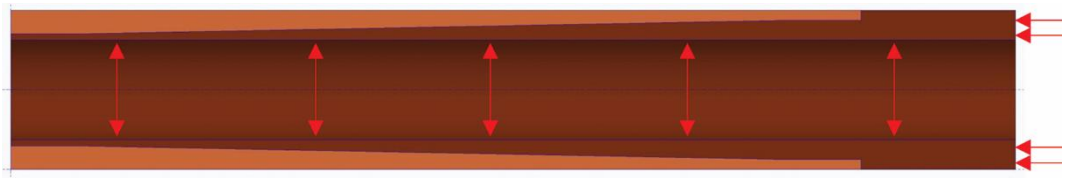

Figure 5. Illustration of phase 1 burnback analysis for the optimized grain

Phase 2. The burning of the slow burning propellant will start at the Phase 2, fig. 6, where the burning slope, replacing the large number of steps present in the original design, will be included. The burning surface area of the fast burning propellant will be similar to the one in the Phase 1. Phase 2 is considered to be finished when the fast burning propellant interior diameter D_f reaches the value set for the diameter of the second step of the slow burning fuel D_{s2}.

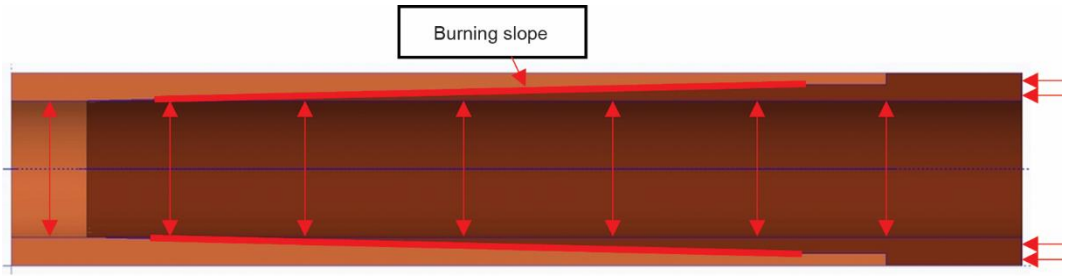

Figure 6. Illustration of Phase 2 burnback analysis for the optimized grain

Phase 3. The fast burning propellant will be totally burned out by the end of this phase as it will continue burning like in the previous phase to the point before starting Phase 4. The formula of A_f is still the same in this phase. The remaining burning surface area relations of this phase are:

$$A_s = \pi L_{s1(k)} D_{s1(k)} + \left\{ \pi [D_{s2(k)} + D_{s1(k)}] \frac{e_{s(k)}}{2} \right\} + \pi L_{s2(k)} D_{s2(k)} + \pi [D_{f(k)} + D_{s2(k)}] \frac{e_{f(k)}}{2} \quad (24)$$

$$e_{s(k+1)} = \sqrt{[L_{slope(k)}]^2 + \left[\left(\frac{D_{s2(k)}}{2} - \frac{D_{s1(k)}}{2} \right) \right]^2} \quad (25)$$

$$L_{slope(k+1)} = L_{slope(k)} + L_{s3(k)} w + w \frac{r_2}{r_1} \quad (26)$$

$$L_{s1(k+1)} = L_{s1(k)} - w \frac{r_2}{r_1} \quad (27)$$

$$L_{f(k+1)} = L_{f(k)} - w \quad (28)$$

$$D_{f(k+1)} = D_{f(k)} + 2w \quad (29)$$

$$D_{s1(k+1)} = D_{s1(k)} + 2w \frac{r_2}{r_1} \quad (30)$$

$$D_{s2(k+1)} = D_{s2(k)} + 2w \frac{r_2}{r_1} \quad (31)$$

$$e_{f(k+1)} = a_{(k)}{}^2 + \sqrt{[c_{(k)} - a_{(k)}]^2} \quad (32)$$

$$a_{(k+1)} = a_{(k)} + w \frac{r_2}{r_1} \quad (33)$$

$$c_{(k+1)} = c_{(k+1)} + w \quad (34)$$

where e_s represents the burning slope as shown in fig. 7, and L_{slope} – the axial slope length.

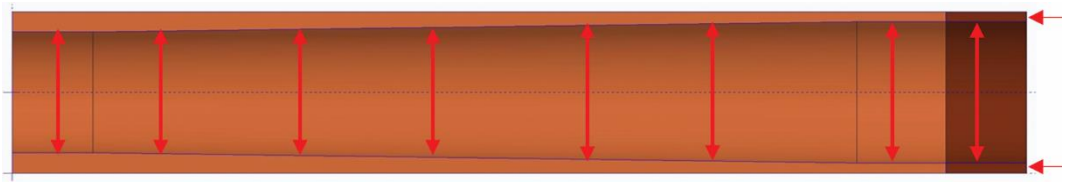

Figure 7. Illustration of Phase 3 burnback analysis for the optimized grain

Phase 4. This Phase consists only of the slow burning propellant, starting with the initiation of the second slow burning propellant step, positioned at the end of the still burning slope. Therefore, A_f will be equal to zero and A_s could be calculated in similar way to Phase 3. This phase is considered to be finished when the diameter of the second step D_{s2} reaches a

value equal to the total diameter, D, of the rocket motor casing, meaning that itis fully burned up. The total burning surface area, during Phase 4, consist of four separate areas, fig. 8. These include the first slow burning step, defined by the diameter D_{s1} and length L_{s1}, the still existing slope L_{slope}, the second slow burning step with the length L_{s2} and diameter D_{s2}, and finally the smaller slope formed during the previous phase e_f.

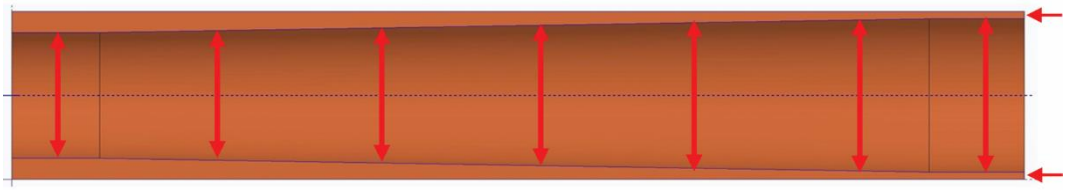

Figure 8. Illustration of Phase 4 burnback analysis for the optimized grain

Phase 5. The last phase represents the last remaining part of the slow burning propellant, fig. 9. The burning surface area of the fast burning propellant will be zero at the beginning of this phase.

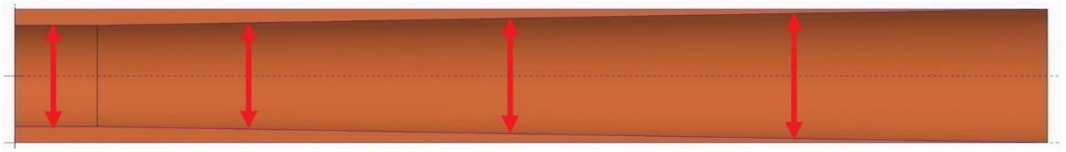

Figure 9. Illustration of Phase 5 burnback analysis for the optimized grain

Experimental results
– Static test of the rocket motor

Static tests are conducted to verify the theoretical performance prediction of SPRM, and to ensure that no defects would occur during the combustion process. Those defects could occur in the form of grain pores and grain cracks because of the internal load pressure, storage, *etc.* [20].

In this investigation, the propellant grains as shown in fig. 10, were produced along with the other rocket motor parts such as the igniter, combustion chamber and nozzle. The assembled SPRM was mounted on a horizontal static test bench [21]. An experimental igniter was used for this test which holds a pressure transducer and load cell, as shown in fig. 11. The measurements were recorded through a data acquisition system.

The data acquisition system is capable to read multiple parameters such as pressure, thrust, temperature and time. It converts the analog signal received from the static test stand to digital values for processing, and it consists of the following components: *sensors* – to convert physical parameters to electrical signals, *signal conditioning circuits* – to convert sensor signals into a form that can be converted to digital values, and *analog-to-digital converters* – to convert conditioned sensor signals to digital values.

The pressure measurement sensor (pressure transducer) is capable of measuring pressure values up to 350 bars. Experimental results are presented in the following section along with theoretical calculations.

Figure 10. A cut out of the original model of the propellant grain

Figure 11. Static test equipment: pressure transducer and load cell

Results and analysis

The results from the developed MATLAB codes were obtained using the same dimensions and characteristics of the experimental rocket motor in order to verify developed analytical models through the comparison with experimental data.

The propellants' characteristics are unified for both grain geometries and they are implemented in the program as input values which are given in tab. 1.

In reference to the technical drawing in fig. 2, the values of the original propellant grain geometric characteristics D, D_f, and L_f are 120 mm, 74.5 mm, and 1260 mm, respectively. Each segment's length L_s is 105 mm, and the diameter of each step was increased by 2 mm. The optimized propellant grain has the same main dimensions, however, the values of D_{s1}, D_{s2}, L_{s1}, L_{s2}, and L_{s3} are 81 mm, 104 mm, 50 mm, 55 mm, and 105 mm, respectively.

Table 1. Propellant characteristics

Parameter	Fast burning propellant	Slow burning propellant
Adiabatic constant, [–]	1.25	1.25
Density, [kgm^{-3}]	1715	1705
Burn rate exponent n, [–]	0.48	0.47
Burn rate coefficient, [ms^{-1}Pa^{-n}]	0.0000101	0.00000855
Burning temperature, [K]	2599.2	2744.6

The MATLAB simulation gives an output in the form of various diagrams, relating to the necessary data for comparing with one another, as well as with the experimental results. Figure 12 shows the burning surface areas of both propellants (slow burning and fast burning), relative to time passed, where it is possible to compare the original and optimized models. While analyzing the change in burning surface area, it is already possible to notice the origin of the initial problem of the SPRM, in the form of gradually forming steps, resulting in reoccurring sudden changes in burning surface area, and henceforth, in the chamber pressure.

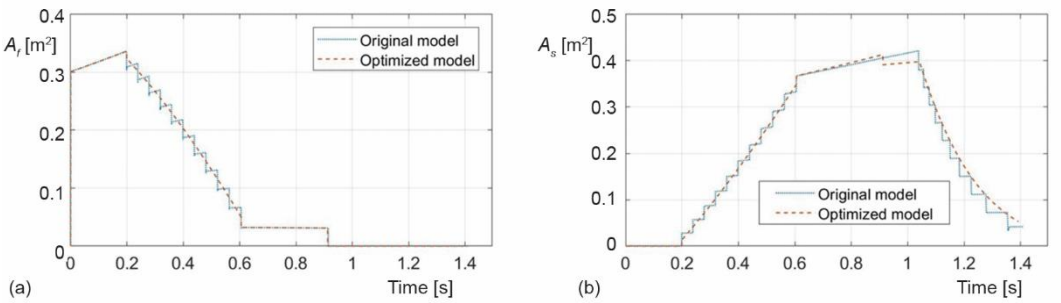

Figure 12. Burning surface area *vs.* time for the original and optimized grain; (a) fast burning propellant area and (b) slow burning propellant area

When compared to the original model, the optimized model shows an almost linear change in burning surface area in the sections previously consisting purely of sharp drops in pressure, whenever a propellant step would end. This occurrence can be noticed during burning of both propellants, as their geometry is codependent.

As expected, the chamber pressure has a similar form to the burning surface area diagram but segmented differently due to the change of propellant and burn rate. The diagram in fig. 13 represents the chamber pressure, the main output of the simulation, and as such is used for comparison with the experimental data, acquired for the nominal initial propellant temperature, equal to 15 °C. It is possible to clearly see that the obtained results for both models align with the experimental results, within the acceptable error margins.

The simulation enables determination of operation pressure for various initial propellant temperatures using eqs. (6) and (7). With the existence of experimental results, not only for 15 °C, but also for extreme working temperatures, the following diagrams were derived for –30 °C, fig. 13(b) and +50 °C, fig. 13(c).

In fig. 13(c), it is possible to see fair alignment between the experimental results and the developed models, showing the accuracy and potential of relatively simple models. The final peak of the optimized model shows lower values of thrust but does not change the general total impulse of the entire SPRM. Unlike to the aforementioned results, fig. 13(b) shows slight deviation between the calculation and experimental data, when analyzing the pressure peaks. This difference extends to less than 10% of the experimental data and can be considered to be within the required margins. Both of these temperature variants give positive results in favor of the analytical models, further proving their adequate accuracy.

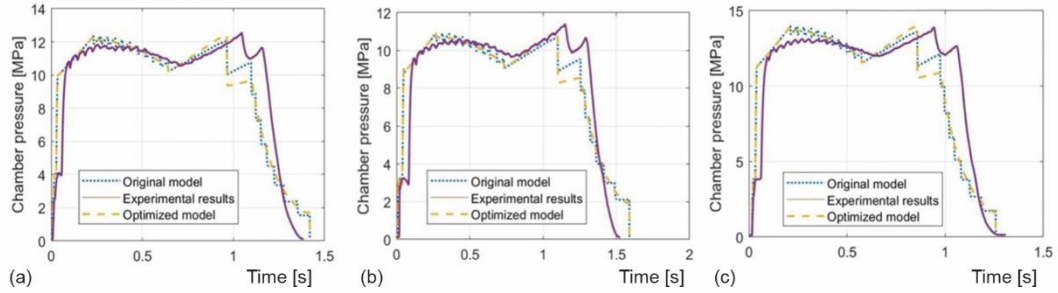

Figure 13. Chamber pressure *vs.* time: comparison between calculated values for original and optimized propellant grain and experimental results at; (a) ambient temperature, 15 °C, (b) cold temperature, –30 °C, and (c) hot temperature, 50 °C

Conclusions

Paper considers application of two-component propellant grain in order to achieve desired pressure and thrust profile with simple cylindrical overall geometry and complex interface area between two propellants. When analyzing the acquired experimental results, it was concluded that there would be a need for an adequate simulation model, not only for further cost efficiency but also for a simpler way of developing further optimized propellant grains. Two geometrical configurations of the grain are thoroughly analyzed and corresponding complex models for burning surface area determination are developed.

After comparing the results of the developed model with the experimental data, it is concluded that the model can successfully be used for simulating the burning process of the propellant. This has created an opportunity for a second model to be developed for an optimized geometry of the propellant grain, with the aim of lowering the oscillations formed during the burning steps between the two propellants. As can be seen, this has provided positive results, all within the required margins of error, allowing for potential production of the new grain.

Further work is aimed at using the developed MATLAB program as a tool to provide a full performance prediction for the rocket motor using the burnback analysis as an initial input, for various two-component propellant grain configuration.

Nomenclature

A – burning surface area, [m^2]
A_f – burning surface area of the fast burning propellant, [m^2]
A_s – burning surface area of the slow burning propellant, [m^2]
A_{se} – burning surface area of the edge, [m^2]
A_t – throat area, [m^2]
a – axial burned edge of the slow fuel, [m]
b – burn rate coefficient, [ms^{-1}Pa^{-n}]
c – radial burned edge of the slow fuel, [m]
c^* – characteristic velocity, [ms^{-1}]
D – outer diameter of both propellants, [m]
D_f – inner diameter of the fast burning propellant, [m]
D_s – inner diameter of the slow burning propellant, [m]
e – length of the burned edge of slow fuel, [m]
e_s – burning slope, [m]
L_f – length of the fast burning propellant, [m]
L_s – length of the segment, [m]
L_{slope} – slope length, [m]
$\dot{m}$ – mass-flow rate, [kgs^{-1}]
n – burn rate exponent, [–]
p_0 – chamber pressure, [Pa]
R – gas constant, [Jkg^{-1}K^{-1}]
r – burning rate, [ms^{-1}]
T_c – burning temperature, [K]
w – burned step, [m]

Greek symbols

ρ_p – propellant density, [kgm^{-3}]
σ_p – temperature sensitivity of burning rate, [K^{-1}]

π – temperature sensitivity of the pressure, [K^{-1}]

References

[1] Sutton, G., Biblarz, O., Solid Propellant Rocket Motor Fundamentals, in: *Rocket Propulsion Elements* John Wiley and Sons Inc., New Jersey, USA, 2016, pp. 434-490
[2] Fabignon, Y., *et al.*, Recent Advances in Research on Solid Rocket Propulsion, *AerospaceLab*, *11* (2016), June, pp. 1-15
[3] Mahjub, A., *et al.*, Design Optimization of Solid Rocket Propulsion: A Survey of Recent Advancements, *Journal of Spacecraft and Rockets*, *57* (2020), 1, pp. 3-11
[4] Bellomi, P., Mancini, V., Solid Propellant Rocket Motor, Patent No. 10359005, AVIO S.P.A., Rome, Italy, 2019, https://patents.justia.com/patent/10359005
[5] ***, The Engine Types: Liquid, Solid and Hybrid ... and a Fourth, NAROM, https://www.narom.no/undervisningsressurser/sarepta/rocket-theory/rocket-engines/the-engine-types-solid-liquid-and-hybrid-and-a-fourth/
[6] Billheimer, J. S., Optimization and Design Simulation in Solid Rocket Design, *Proceedings*, ICRPG/AIAA 3rd Solid Propulsion Conference, Atlantic City, N. J., USA, 1968, no. 86-488, pp. 1-10
[7] Reddy, K. O., Pandey, K. M., Burnback Analysis of 3-D Star Grain Solid Propellant, *International Journal of Advanced Trends in Computer Science and Engineering*, *2* (2013), 1, pp. 215-223
[8] Oh, S. H., *et al.*, Study on Solid Propellant Grain Burnback Analysis Applying Face Offsetting Method, *Journal of the Korean Society of Propulsion Engineers*, *23* (2019), 4, pp. 81-91
[9] Stalin, P., Design and Geometrical Analysis of Propellant Grain Configurations of a Solid Rocket Motor, *International Journal of Engineering Development and Research*, *2* (2014), 4, pp. 3417-3427
[10] Puskulcu, G., Ulas, A., 3-D Grain Burnback Analysis of Solid Propellant Rocket Motors: Part 1 – Ballistic Motor Tests, *Aerospace Science and Technology*, *12* (2008), 8, pp. 579-584
[11] Puskulcu, G., Ulas, A., 3-D Grain Burnback Analysis of Solid Propellant Rocket Motors: Part 2 – Modelling and Simulations, *Aerospace Science and Technology*, *12* (2008), 8, pp. 585-591
[12] Živković, S., *et al.*, Experimental Determination of Rocket Motor Internal Ballistic Coefficients and Performance Parameters, *Proceedings*, OTEH 2014: 6th International Scientific Conference on Defensive Technologies, Belgrade, Serbia, 2014, pp. 289-295
[13] Gossant, B., Solid Propellant Combustion and Internal Ballistics, in: *Solid Rocket Propulsion Technology* (Ed. A. Davenas), Pergamon Press, New York, USA, 1993, pp. 111-192
[14] Javed, A., *et al.*, Internal Ballistic Code for Solid Rocket Motors Using Minimum Distance Function for Grain Burnback, *Defence Science Journal*, *65* (2015), 3, pp. 181-188
[15] Thunaipragasam, S., Natarajan, K., Experimental Study on Composite Solid Propellant Material Burning Rate Using Algorithm MATLAB, *Thermal Science*, *20* (2016), suppl. 4, pp. 1119-1125
[16] Selvakumaran, T., Kadiresh, N., Investigation on Parameters Influence for Intrinsic Instability Analysis of Solid Propellant (AP+HTPB+TDI) Using Computational Image-Processing Technique, *Thermal Science*, *22* (2018), 6B, pp. 3003-3009
[17] Kamran, A., Liang G., Design and Optimization of 3-D Radial Slot Grain Configuration, *Chinese Journal of Aeronautics*, *23* (2010), 4, pp. 409-414
[18] Kamran, A., Liang G., An Integrated Approach for Optimization of Solid Rocket Motor, *Aerospace Science and Technology*, *17* (2012), 1, pp. 50-64
[19] Raza, M. A., Liang, W., Design and Optimization of 3-D Wagon Wheel Grain for Dual Thrust Solid Rocket Motors, *Propellants, Explosives, Pyrotechnics*, *38* (2013) 1, pp. 67-74
[20] Fan, J., Tan, F., Analysis of Major Defects and Nondestructive Testing Methods for Solid Rocket Motor, *Applied Mechanics and Materials*, *365-366* (2013), Aug., pp. 618-622
[21] Soares, D. M., *et al.*, Development of a Vertical Static Test Bench for Amateur Rocket Engines, *International Journal of Advanced Scientific and Technical Research*, *5* (2018), 8, pp, 45-49

Paper submitted: June 4, 2021
Paper revised: August 19, 2021
Paper accepted: August 20, 2021